A STEPWISE, ITERATIVE PROCEDURE TO CONSTRAIN STRESS DROP, REGIONAL ATTENUATION MODELS, AND SITE EFFECTS

Mark D. Fisk[1] and W. Scott Phillips[2]

Alliant Techsystems[1] and Los Alamos National Laboratory[2]

Sponsored by Air Force Research Laboratory[1] and National Nuclear Security Administration[2]

Contract Nos. FA8718-09-C-0005[1] and LA09-BAA09-01-NDD03[2]

ABSTRACT

Accurate corrections for attenuation, geometrical spreading, source size, and site effects are needed for reliable use of regional seismic phases for discrimination and magnitude estimation. Without constraints, the full parameter space has many tradeoffs and instabilities that can lead to significant errors. We are developing a stepwise, iterative procedure, utilizing constraints, to provide more accurate parameter estimates. As a starting point, we use spectral ratios of regional phases for nearby events of different moments to eliminate path and site effects, yielding more reliable estimates of the source parameters. As shown by Schaff and Richards (2004) and Fisk et al. (2008), there are many pairs of nearby similar events throughout Eurasia available for this analysis. We then correct the spectra for source effects to be able to estimate more reliable distance and site corrections, adopting this same basic approach to constrain remaining tradeoffs. A key element of this effort is incorporation of coda envelope measurements, along with spectra of direct regional phases. The stability of coda allows the analysis to be applied to event pairs that are non-similar and may be separated by, e.g., up to 50 km, greatly augmenting those that can provide accurate source terms. We have acquired from IRIS a very large dataset of three-component regional seismic recordings for events listed in the USGS PDE from 1989 to 2009 that have epicenter estimates within 50 km of another event, with at least 0.7 magnitude units difference, and the larger event of each pair at least mb 5. The set includes over 46,000 such pairs, corresponding to about 9,400 unique events. We have processed 599,226 waveforms to compute spectra of direct Pn, Pg, Sn, and/or Lg phases (of the order of 2,000,000 spectra) and coda envelopes in 16 frequency bands (about 10,000,000 envelopes). We have computed and fit a relative Brune (1970) source model to network-median relative spectra for all 46,000 pairs. We have reviewed and compared relative spectra and model fits for direct phases and coda to assess the reliability of the estimated source parameters, the dependence on station coverage and event similarity, and effects of various data quality issues. We present several cases, corroborating the stability of coda, showing very comparable source terms estimated from coda and direct-phase for many, even for single stations for well-recorded, similar event pairs, and good agreement with available published studies that used dense local networks. The comparisons also highlight the complementary benefit of using multiple, independent measurements of coda and direct phases, which have led to improvements in the processing both (e.g., better fitting methods, restricting the data to those of higher quality using a magnitude-distance criterion, and flagging discrepancies, often due to data quality issues, for review). These collective processing and review efforts have led to a large, reliable set of source terms. We then show how the source-corrected spectra are used to estimate distance and site corrections. We also plan to use coda measurements to independently estimate and validate the site terms. We describe plans to partition the uncertainties and their correlation lengths for use in Bayesian methods to interpolate grids of stress drop, geometrical spreading, and Q estimates, and to merge our results with previous developments at Los Alamos National Laboratory (LANL).

OBJECTIVES

We are developing, applying, and evaluating methods to improve the accuracy of attenuation models, geometrical spreading, site terms, and their uncertainties for regional phases in Eurasia, by constraining trade-offs among the parameters at various stages of the analysis. The approach is to break up traditional grid-search inversions, which are known to have many trade-offs and instabilities (cf. Fisk and Phillips, 2009), into manageable pieces, canceling out certain physical effects (e.g., distance and site) to allow reliable estimation of others (e.g., source), and then correcting for the latter to then estimate reliable parameters for the former. We are processing spectra of direct phases and coda envelope measurements to augment and corroborate source terms and to independently estimate site terms. We also plan to use multiple methods to estimate the correction parameters and to validate the results at key stages. We plan to partition the uncertainties and their correlation lengths, interpolate grids of stress drop, geometrical spreading, and Q estimates, and merge our results with amplitude tomography developments at LANL. We will evaluate the corrections and uncertainties using two large datasets and cross-validation methods.

RESEARCH ACCOMPLISHED

Following Sereno et al. (1988), Taylor and Hartse (1998), Taylor et al. (2002), and numerous others, the amplitude spectrum for a given phase and station, for event i, may be modeled by

$$A_i(f) = S_i(f; M_0, f_c(\sigma_b^{(0)}, \psi)) G(r_i; r_0, \eta) \exp\left(-\frac{\pi f^{1-\gamma}}{Q_0 \nu} r_i\right) P(f; a, b) \quad , \qquad \text{(EQ 1)}$$

where $S_i(f)$ is the source spectrum with seismic moment M_0 (and radiation pattern terms) and corner frequency f_c (which may be parameterized in terms of M_0, stress drop $\sigma_b^{(0)}$ or apparent stress, and a scaling parameter ψ), r_i is epicentral distance, $P(f)$ is a frequency-dependent site term, $Q_0 f^{\gamma}$ represents anelastic attenuation, ν is group velocity, and $G(r, r_0)$ represents frequency-independent geometrical spreading, inversely proportional to distance to a power η, beyond a reference distance r_0. The objective is to accurately estimate the parameters shown in red.

Constrained Inversion Approach

Instead of performing a grid search for all parameters simultaneously, we start by using relative spectra for event pairs with similar locations and focal mechanisms (assessed by waveform cross-correlations), but different moments, to factor out path and site effects and obtain reliable estimates of the source terms. Once accurate source terms are estimated, the source-corrected spectra can be used to estimate the distance and site terms. That is, for a pair of nearby earthquakes with similar radiation patterns, the relative spectra for a given seismic phase type is modeled by

$$\frac{A_1(f)}{A_2(f)} = \frac{S_1(f)}{S_2(f)} = \frac{M_0^{(1)}[1 + (f/f_c^{(2)})^2]}{M_0^{(2)}[1 + (f/f_c^{(1)})^2]} \quad . \qquad \text{(EQ 2)}$$

This approach requires many similar pairs. Schaff and Richards (2004) showed that there are indeed many such pairs. In addition, Mayeda et al. (2007) showed that coda is less sensitive to focal mechanism, event separation, and station coverage. This allows the requirement of similar events to be relaxed, greatly augmenting the number of pairs for which source terms can be estimated. Thus, in addition to using relative spectra of direct regional phases, we compute coda envelopes, using the processing method as Mayeda et al. (2003) and Phillips et al. (2008). We then compute a pseudo relative spectrum as the median ratio of coda envelopes in 16 frequency bands. For example, Figure 1 shows relative spectra of Pn, Sn, Lg, and coda, along with source model fits for an earthquake pair. Note that the relative coda spectrum, just using MK31 three-component (3C) data, is nearly the same as the network results for coda and direct phases using 19 regional stations. Spectra of direct phases and coda envelopes each have distinct advantages (discussed further below); their independence corroborates estimated source terms or helps identify problems.

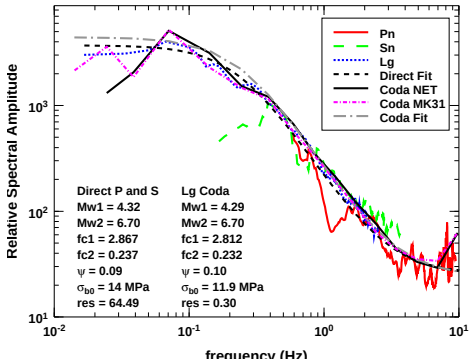

Figure 1. Network-median relative spectra of Pn, Sn, Lg, and Lg coda (using 19 stations and just MK31) for an event pair in southwestern Siberia. Model fits and estimated source parameters agree very well.

As an initial comparison, we estimated source terms from direct phases and coda for a cluster of about 100 events in southern Russia. Figure 2 shows that the estimates of moments and corner frequencies are similar. To assess the reliability of the resulting path corrections using these independent source estimates, we corrected Lg spectra at 23 stations using source estimates from direct phases or coda. Figure 3 shows the source-corrected Lg spectra at BRVK, along with fits of the combined site and distance terms. Figure 4 compares Q estimates, showing that the results using source terms from coda or direct phases are highly correlated. We have yet to treat site effects, so these estimates will likely change, but the relative corrections, using independent source estimates from coda and direct phases, are very consistent.

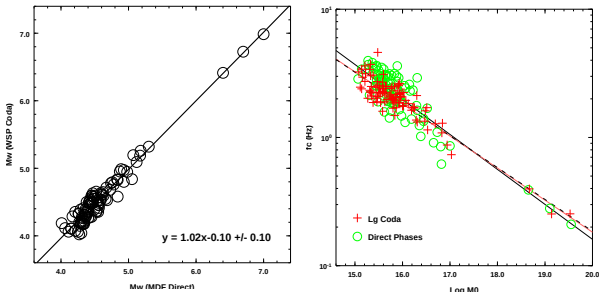

Figure 2. Comparison of Mw estimates (left) and corner-frequency scaling (right), independently estimated from direct phases and Lg coda.

Large-Scale Processing

We acquired regional data from IRIS for events listed in PDE from 1989 to 2009 that have epicenter estimates within 50 km of another event, a magnitude difference of at least 0.7 m.u., and the larger event of each pair at least mb 5. The set includes 46,495 such pairs, corresponding to 9,395 unique events, shown in Figure 5. Also shown are IRIS stations and ray paths with data, indicating good coverage for much of Eurasia. Unlike tomography, our approach does not require crossing ray paths to estimate model parameters of Eq. (1), providing constraints for many paths and extending calibration to the edges of Eurasia (e.g., Russia, India, and the Arabian Peninsula). We automatically processed about 2,000,000 spectra of regional phases and about 10,000,000 coda envelopes, computed network-median relative spectra, and fit Eq. (2) to over 46,000 pairs, without restricting to similar event pairs. We computed waveform cross-correlations for all pairs that can be used to assess the similarity of mechanisms for cases where results from direct phases and coda disagree. We have reviewed the results for master events of mb 5.5 and larger and are completing the review for the remaining master events.

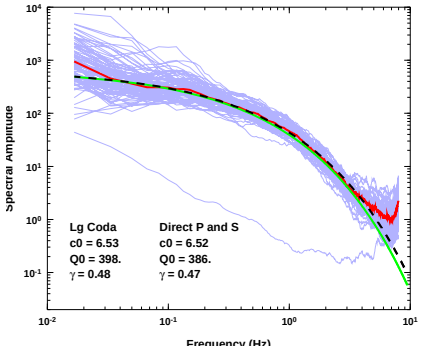

Figure 3. Source-corrected Lg spectra at BRVK for 100 events in the cluster (blue), the median (red), and Q model fits (black dashed and green) using source corrections from direct phases and coda, respectively.

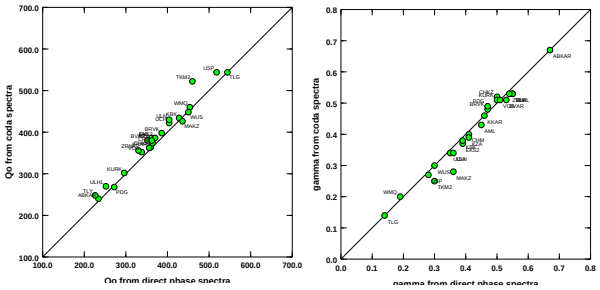

Figure 4. Comparison of Q_0 (left) and γ (right; exponent of frequency-dependent Q) estimates from coda versus direct phases, showing good agreement.

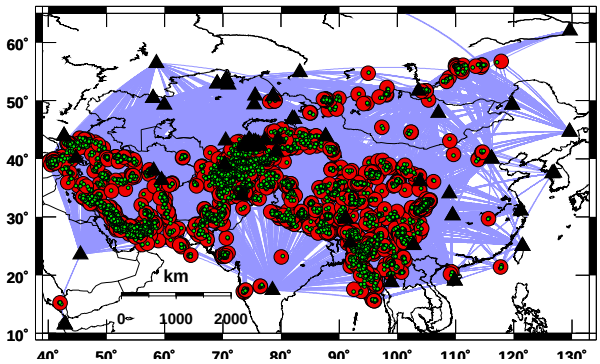

Figure 5. Map of earthquakes listed in the PDE from 1989 to 2009; red circles correspond to mb>5 events within 50 km of smaller events (green circles). Also shown are ray paths for which regional seismic data are available from IRIS stations (triangles).

Figure 6 compares preliminary estimates of source parameters from direct phases versus coda. Moments of the large master events are fixed, using values in the PDE; they were not used in the linear regression (left plot), which shows very good overall agreement. There are clearly discrepancies, particularly for the corner frequencies, which we are investigating/reconciling.

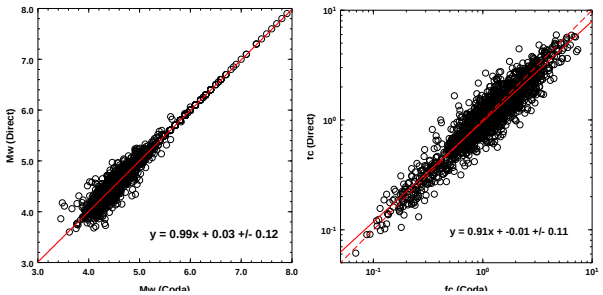

Figure 6. Preliminary estimates of Mw and corner frequency from direct phases versus coda.

Detailed Examinations

Because automatic processing is needed for this very large data set, to build confidence in the procedure and the resulting source terms, we compared coda and direct results in detail for many cases and to published results. Here we show some that highlight the dependence of the results on station coverage and the benefits of using both direct phases and coda. For example, coda results at even a single station are often comparable to network results, as illustrated in Figure 1. Since not all pairs are equally well recorded or similar, an important question is how sensitive direct-phase results are. We examine this for progressive cases, starting with an ideal one. Figure 7 shows the locations of a large, similar pair recorded by 19 stations within 14º. The left plot of Figure 8 shows the network-median relative spectra and source model fits for this pair. The coda and direct Lg relative spectra are remarkably similar, even for subtle Lg fluctuations above 1 Hz. It can be argued that the direct-phase results are so consistent because the events were well recorded. However, the right plot of Figure 8 shows that the coda and direct results also agree just using station CHKZ. Figure 9 shows estimated corner frequencies versus log moment for each of 19 stations. Except for data quality issues at three stations for coda and one for direct Lg, the single-station results agree very well. Clipping at MK31 for the Mw 6.7 event has a greater effect on direct Lg, leading to a discrepancy (Figure 10). Data quality issues at a small fraction of stations do not impact the network median, but could affect the results if recorded by fewer stations. The discrepancy of source terms from coda and direct phases can flag such problems, without having to examine many thousands of waveforms.

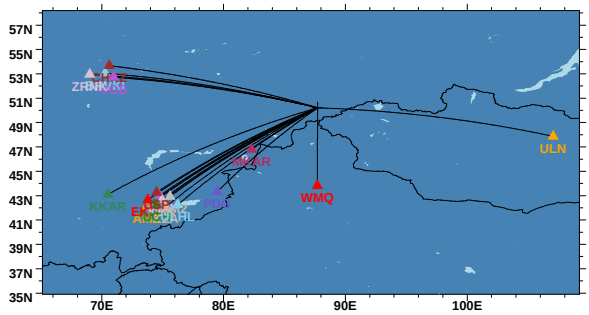

Figure 7. Locations of an event pair in southern Russia and regional stations with recordings.

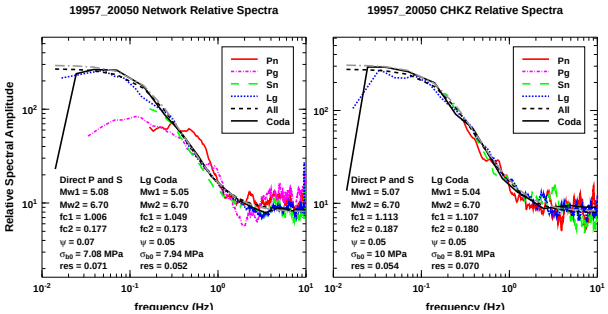

Figure 8. Relative spectra from direct phases and Lg coda, and source model fits and parameter estimates using 19 stations (left) and just using CHKZ (right).

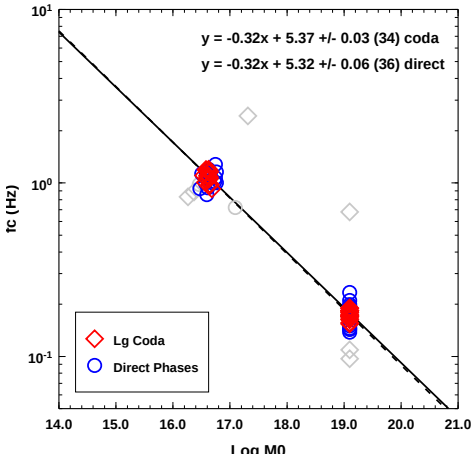

Figure 9. Single-station estimates of corner frequency versus log moment and scaling relations (linear fits) from direct phases and Lg coda. Gray markers correspond to stations with data quality problems.

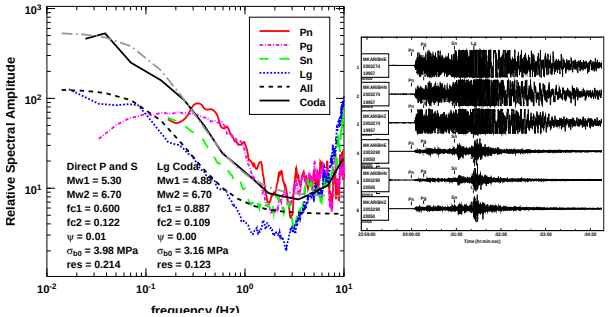

Figure 10. Relative spectra from direct phases and Lg coda at MK31 (left), which disagree due to clipping for the larger event (right).

As a less ideal case, Figure 11 depicts two earthquakes at the Lop Nor test site (LNTS), smaller (Mw 5.5/4.2) than the first case and recorded out to 20º. Figure 12 shows relative spectra at MAKZ and NIL. For NIL, the direct-phase results agree with MAKZ and network results. Lg coda has poor SNR for this path, illustrating how direct P and S phases complement coda. Figure 13 shows single-station estimates of corner frequencies versus moment. Coda results have less scatter, but the direct-phase results are similar. Figure 14 shows single-station f_c estimates versus distance. Even requiring SNR>3, data quality degrades for longer paths/smaller events, causing biases and apparent distance dependence. Using a magnitude-distance criterion (e.g., Phillips et al., 2008) to restrict the data to higher quality generally improves the results, as illustrated in Figure 15 for LNTS.

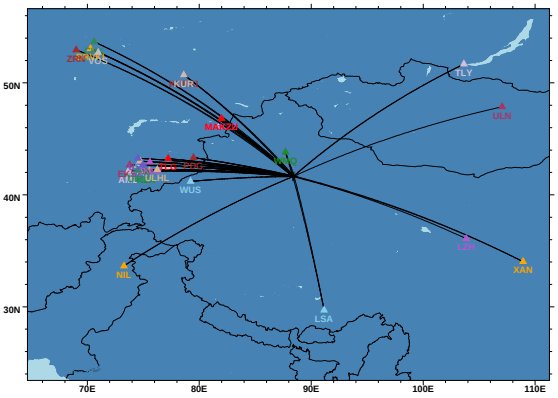

Figure 11. Locations of an earthquake pair during January 1999 at LNTS and regional stations.

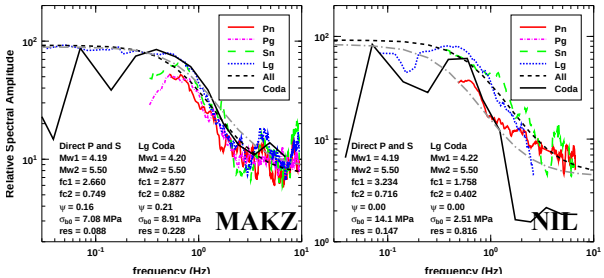

Figure 12. Relative spectra and source model fits at MAKZ (left) and NIL (right) for the LNTS pair.

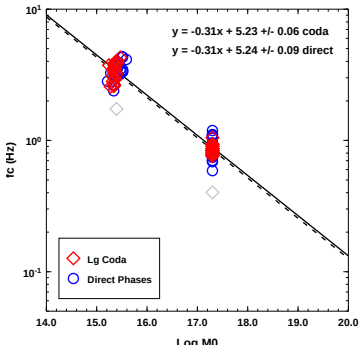

Figure 13. Estimates of corner frequency versus log moment from direct phases and Lg coda at each station using a pair of events at LNTS. The NIL coda result is an outlier.

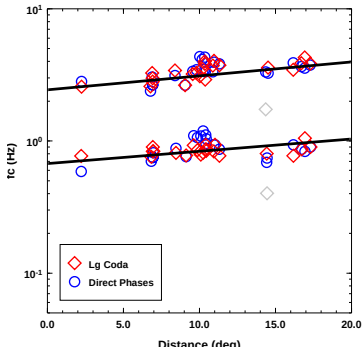

Figure 14. Single-station estimates of corner frequency versus distance to each station for the LNTS pair, showing apparent trends.

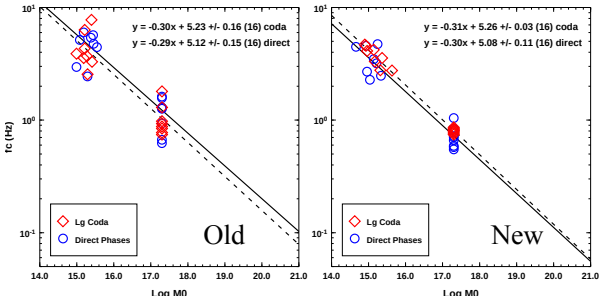

Figure 15. Source parameter estimates for 8 crustal pairs near LNTS using all regional data (left) and restricting the data by magnitude/distance (right).

A sequence of Bhuj earthquakes is interesting because: (1) IRIS data are available from only 3 regional stations (Figure 16); (2) direct Lg is clipped at HYB for the main shock; (3) one NIL channel is missing; (4) Lg does not propagate efficiently to ABKT (Δ = 1980 km); and (5) many aftershocks occurred throughout the crust. Thus, this is a case of very limited data and source variability. Figure 17 shows relative spectra for one pair, using only NIL data for direct Lg, and NIL and HYB data for Pn, Sn and coda. The magnitude-distance criterion excludes ABKT for all but the largest events. Figure 18 shows estimates of source parameters. From the fits, using 1-3 regional stations, we estimate fc = 0.072, 0.084 Hz for the main shock from coda and direct phases. Using 8 local stations, Bodin and Horton (2004) estimate static stress drop of 16-20 MPa, giving fc = 0.066-0.071 Hz. Thus, using very limited data, our results are consistent with GT source information. The scatter and bias for the smaller events (Figure 18) are due to a combination of varying locations, depths, mechanisms, and SNR effects.

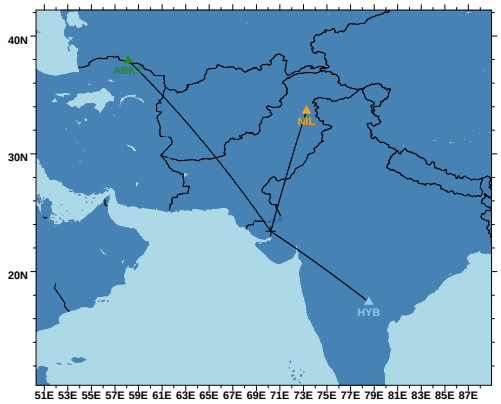

Figure 16. Locations of Bhuj, India earthquakes with regional recordings by ABKT, HYB, and NIL.

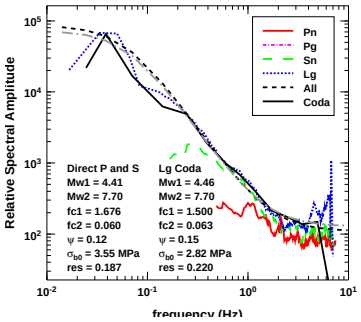

Figure 17. Relative spectra and model fits for a Bhuj pair, using NIL data for direct Lg and NIL and HYB data for other phases.

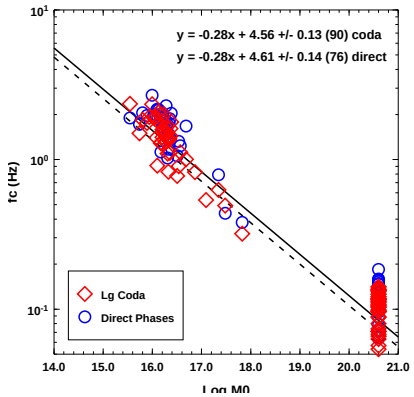

Figure 18. Estimates of f_c versus log M_0 for Bhuj events. Linear regressions were weighted by moment.

I also processed a pair of earthquakes near Wells, NV that are reported to have strong source directivity. They were recorded by several permanent broadband networks and 400 portable broadband USArray stations with 70-km spacing. Using stations at more typical regional distances (Figure 19), 22 with good data, Figure 20 (left) shows that network-median relative spectra from direct phases and coda agree quite well, even for Pn (often the most variable) over frequencies with adequate SNR. Our Mw estimates of 4.27 and 4.29 for the smaller event, fixing Mw 5.8 for the larger, agree with estimates of 4.3 and 5.8 by Mendoza and Hartzell (2009), who used a finite-fault method. They estimated static stress drop of 7.2 MPa for the larger event, noting that it is higher than expected for the Basin and Range, equivalent to f_c = 0.39 Hz. I obtain f_c estimates of 0.29-0.31 Hz from coda and direct phases.

There are many cases for which the source parameters estimated from coda and direct phases agree very well, typically for event pairs with similar mechanisms. It is also interesting to examine discrepancies of coda and direct results. Figure 21 depicts the location of one such cluster of 10 events in Kazakhstan, near the Caspian Sea.

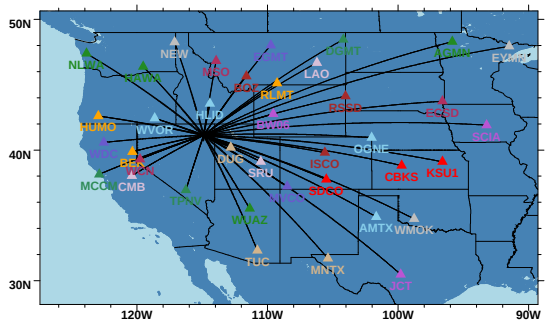

Figure 19. Locations of earthquakes near Wells, Nevada and 39 stations at regional distances.

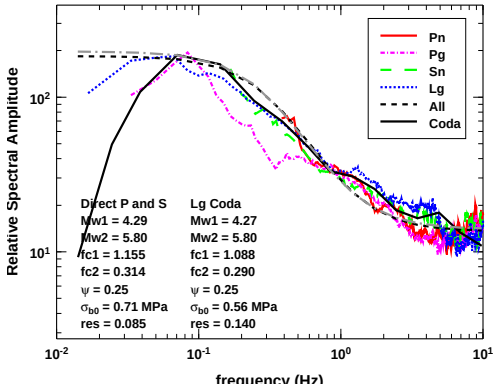

Figure 20. Relative spectra, model fits, and source parameter estimates for a pair of Wells earthquakes.

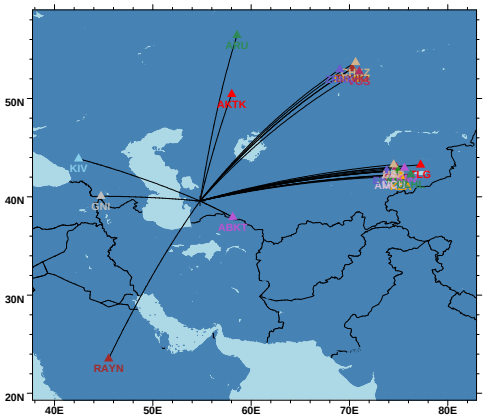

Figure 21. Locations of a cluster of earthquakes near the Caspian Sea and recording regional stations.

Figure 22 (left) shows corner frequency estimates versus log M_0 from all 10 pairs; the direct-phase results exhibit much more scatter and bias than coda. Figure 22 (right) shows the results for the events with waveform cross-correlations greater than 0.6. The coda results are very similar in both cases, illustrating its stability to source effects. The direct-phase results have much less scatter and bias by restricting to similar pairs.

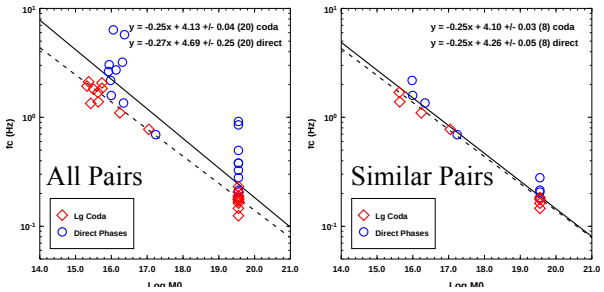

Figure 22. Estimates of source parameter for a cluster in Kazakhstan, using 10 events within 50 km of the master (left) and restricting the events to those with similar waveforms/mechanisms (right).

As a final case, Figure 23 depicts a cluster in Myanmar. Figure 24 shows estimates of corner frequencies versus log moment using up to 5 stations; 5 of 11 coda results are outliers due to data quality issues. When excluded, the coda results are tighter than those from direct phases, as seen for many cases, but can be more prone/sensitive to data quality problems because measurement windows are longer, increasing the probability of including spurious signals, and SNR is lower than direct Lg.

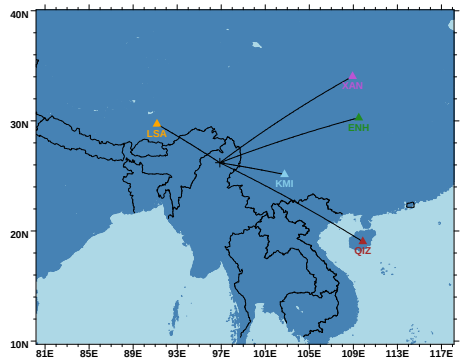

Figure 23. Location of an Mw 5.9 earthquake in Myanmar and 5 regional stations with recordings.

For example, an Mw 5.0 event occurred 13 minutes after the largest (Mw 5.9); its signals are in the coda of the preceding event (Figure 25), which biases the estimates of source parameters for both events of the pair. The corner-frequency estimates from coda for this pair are the most inconsistent with all of the other results. The results from direct Lg are also biased some, but not nearly as much because it has higher SNR.

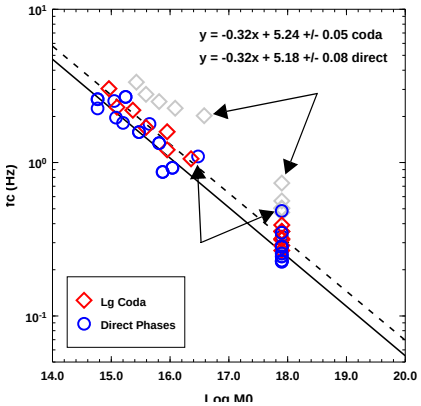

Figure 24. Estimates of corner frequency versus log moment and scaling relations from direct phases and Lg coda, using data from up to five common stations. Gray markers are outliers of the coda results.

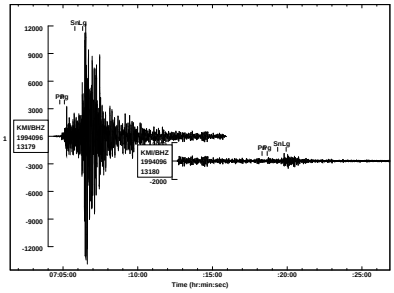

Figure 25. KMI data for two events in the Myanmar cluster, separated in time by about 13 minutes.

Comparisons of Preliminary Q Parameters

Now that we are establishing a large set of corroborated source terms, the next step is to fit the source-corrected spectra to estimate the distance and site terms. For paths from LNTS to regional stations, we compared our Q_0 estimates for Pn, Sn, Lg to those computed as averages of Q_0^{-1} along the paths from tomography by Dr. Phillips. Our results were generated using only one pair at LNTS. Figure 26 shows examples of source-corrected spectra for various phases and fits, giving estimates of effective Q parameters. Figure 27 compares Lg Q_0 estimates for 24 stations, which agree well for stations in Kazakhstan and Kyrgyzstan. Our average Lg Q_0 for these paths is 442 versus 478 from tomography. Our Lg Q_0 estimates are 18-32% lower than those from tomography for TLY, NIL, LZH, ULN, and WMQ, paths for which stations are sparse. We are using more data to improve and validate these initial results. It is interesting that we obtain similar results for many stations using a single pair with well-constrained source terms, which can be used to constrain tomography, particularly for paths with sparse coverage.

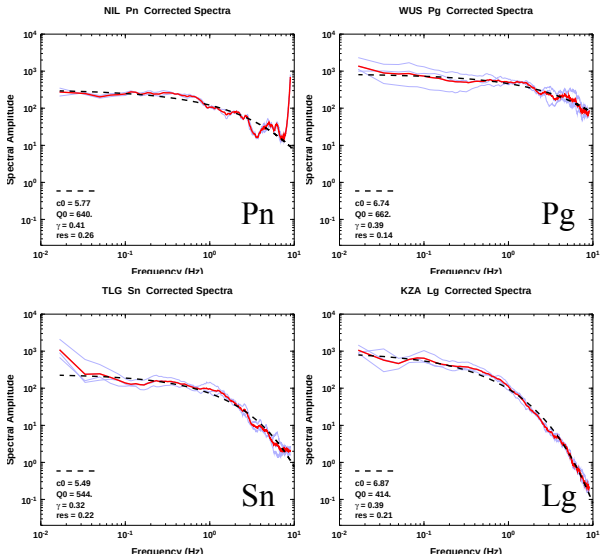

Figure 26. Examples of source-corrected spectra and Q model fits using a pair of LNTS earthquakes.

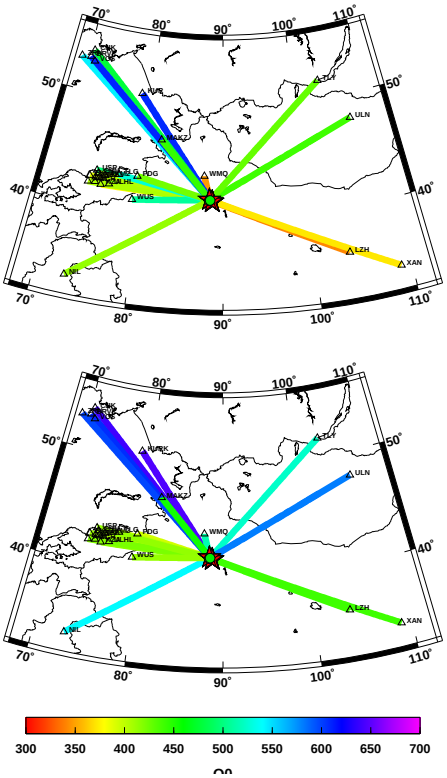

Figure 27. Effective Lg Q_0 for paths from LNTS to regional stations from our analysis (top) and based on amplitude tomography (bottom).

Figure 27 shows effective Lg Q_0 estimates for selected paths to MAKZ and MKAR, illustrating systematic path variations. We still need to treat frequency-dependent site effects, which will affect the Q estimates; however, the estimates of source terms and Q for these paths can help constrain amplitude tomography work at LANL, providing the most immediate benefit to existing efforts.

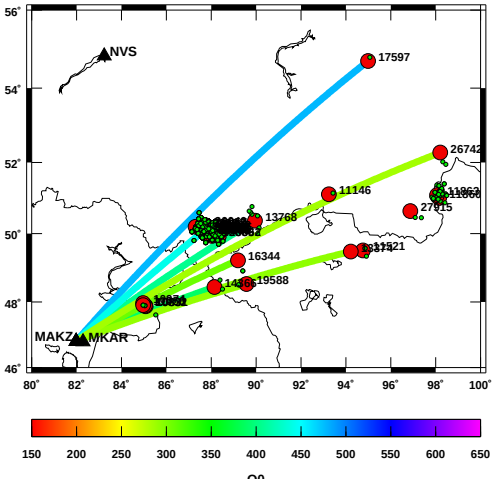

Figure 28. Effective Lg Q_0 for paths to MAKZ and MKAR, using source corrections estimated from various pairs/clusters.

Next Steps

By first eliminating path and site effects, using an EGF approach, accurate source terms can be estimated for events with suitable data. These terms and fits of source-corrected spectra (e.g., Figure 26) completely calibrate all combined physical effects over a broad spectral range for relevant paths. For isolated clusters, the fits do not provide independent estimates of Q, spreading, and site parameters. We are extending the constrained approach to eliminate remaining trade-offs. For example, site effects have frequency dependence that, if inaccurately treated, can adversely impact Q estimates. An approach that imposes a constraint is to use relative spectra for clusters with similar paths, but different distances from a station, to factor out the site term and estimate of Q for that path. Figure 29 illustrates this approach. It shows the ratio of the median source-corrected spectra for two clusters along a path to MAKZ. This factors out the site term, and the spreading terms are different constants, independent of frequency. Thus, the estimate of Q has no trade-off with source, site, or geometrical spreading effects. Assuming the effective Q is relatively constant over a path, the ratio of source-corrected median spectra for the two clusters is simply modeled by

$$\log(\tilde{A}_1/\tilde{A}_2) = \frac{\pi f^{1-\gamma}}{Q_0 v}\Delta r \ , \qquad \text{(EQ 3)}$$

where Δr is the separation of the clusters. Fitting this expression to empirical spectral ratios (dashed curve in Figure 29) gives constrained estimates of Q_0 and γ (e.g., Lg $Q_0 = 546$) for the path.

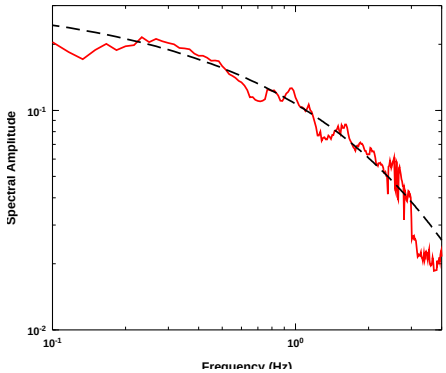

Figure 29. Ratio of source-corrected median spectra for two clusters along a great-circle path to MAKZ. The relative spectrum factors out the site term and allows a robust estimate of Q for this path.

Now correcting the source-corrected spectra for Q, the remaining frequency dependence is due to site effects. Once this is done for at least one path, the frequency-dependent site term may be estimated and fixed, under a typical assumption that $P(f)$ is independent of azimuth. We can then estimate Q for all paths with available data. The other assumption is that a suitable path exists for a given station along which Q is fairly constant. We are investigating its validity for stations of interest.

CONCLUSIONS AND RECOMMENDATIONS

We are developing and testing methods to constrain source, distance, and site corrections for regional phases. We have processed 20 years of IRIS data for Eurasia. A significant aspect has been incorporating coda measurements to corroborate, augment, and improve source estimates from direct phases. Coda is generally more stable, allowing estimates for more pairs that do not have similar mechanisms or that are not as well recorded. Source terms estimated from relative coda envelopes

generally have lower variance than those from spectra of direct phases. However, they often compare very well, even for single stations, for similar pairs with good data. Our results also agree with published studies based on dense local networks, for the Bhuj cluster with very limited regional data and for Wells events that have source directivity effects. Examples shown highlight that direct phases can be variable for non-similar event pairs and coda results can be more prone to data quality issues. Note that processing a data set of this size requires a high degree of automation; it is impractical to examine all of the data. Agreement of the coda and direct-phase results help to validate the source terms. Discrepancies flag various (e.g., data quality) problems that need to be treated. Because reliable source terms are an important foundation for this effort, significant efforts have been made to compare coda and direct results and improve the processing of both. We plan to finish reviewing the source terms and quantify their uncertainties.

Amplitude tomography is a major, ongoing calibration effort at LANL. Our source terms can be used in the near term as quasi ground truth for tomographic inversions, both to validate existing grids and to improve them by imposing constraints. We plan to use cross-validation methods to start testing improvements to tomographic grids. We also plan to progress to the next phase of this project, using source-corrected spectra and additional constraints (e.g., as illustrated by Eq. (3) and Figure 29) to estimate reliable path and site terms. Other key aspects of this work are to partition the uncertainties, validate the distance and site corrections, and also merge them with amplitude tomography.

ACKNOWLEDGMENTS

Seismic data from IRIS were used in this study.

REFERENCES

Bodin, P., and S. Horton (2004). Source parameters and tectonic implications of aftershocks of the Mw 7.6 Bhuj earthquake of 26 January 2001, *Bull. Seismol. Soc. Am.*, 94: 818–827.

Bodin, P., L. Malagnini, and A. Akinci (2004). Ground-motion scaling in the Kachchh Basin, India, deduced from aftershocks of the 2001 Mw 7.6 Bhuj earthquake, *Bull. Seismol. Soc. Am.*, 94: 1658–1669.

Brune, J. N. (1970). Tectonic stress and the spectra of seismic shear waves from earthquakes, *J. Geophys. Res.*, 75: 4997-5009.

Fisk, M. D., G. D. McCartor, and S. R. Taylor (2008). Robust Magnitude, Distance, and Path-Specific Corrections for Regional Seismic Phases by Constrained Inversion and Enhanced Kriging Methods, ATK/NCR-0608-501, Final Report.

Fisk, M. D. and W. S. Phillips (2009). A Stepwise, Iterative Procedure to Constrain Stress Drop, Regional Attenuation Models, and Site Effects, in *Proceedings of the 2009 Monitoring Research Review: Ground-Based Nuclear Explosion Monitoring Technologies*, LA-UR-09-05276, Vol. 1, pp. 52-61.

Mayeda, K. M., A. Hofstetter, J. L. O'Boyle, and W. R. Walter (2003). Stable and Transportable Regional Magnitudes Based on Coda-Derived Moment-Rate Spectra, *Bull. Seismol. Soc. Am.*, 93: 224-239.

Mayeda, K. M., L. Malagnini, and W. R. Walter (2007). A new spectral ratio method using narrow band coda envelopes: evidence for non-self-similarity in the Hector Mine sequence, *Geophys. Res. Lett.*, 34: L11303.

Mendoza, C., and S. Hartzell (2009). Source analysis using regional empirical Green's functions: The 2008 Wells, Nevada, earthquake, *Geophys. Res. Lett.*, 36, L11302, doi:10.1029/2009GL038073.

Phillips, W. S., R. J. Stead, G. E. Randall, H. E. Hartse and K. Mayeda (2008). Source effects from broad area network calibration of regional distance coda waves, in *Scattering of Short Period Waves in the Heterogeneous Earth*, H. Sato and M.C. Fehler, Editors.

Schaff, D. P. and P. G. Richards (2004). Repeating seismic events in China, *Science*, 303: 1176-1178.

Sereno T. J., S. R. Bratt and T. C. Bache (1988). Simultaneous inversion of regional wave spectra for attenuation and seismic moment in Scandinavia, *J. Geophys. Res.*, 93: 2019-2035.

Taylor, S. R., and H. E. Hartse (1998). A procedure for estimation of source and propagation amplitude corrections for regional seismic discriminants, *J. Geophys. Res.,* 103: 2781-2789.

Taylor, S. R., A. A. Velasco, H. E. Hartse, W. S. Phillips, W. R. Walter, and A. J. Rodgers (2002). Amplitude corrections for regional seismic discriminants, *Pure and Appl. Geophys.*, 159: 623-650.